Study of crankshaft torsional deformation under steady-state and transient operation of turbocharged diesel engines

E G Giakoumis, C D Rakopoulos*, and A M Dimaratos
Department of Thermal Engineering, School of Mechanical Engineering, National Technical University of Athens, Athens, Greece

The manuscript was received on 24 May 2007 and was accepted after revision for publication on 6 December 2007.

DOI: 10.1243/14644193JMBD113

Abstract: The modelling of transient operation of turbocharged diesel engines appeared in the early 1970s, and continues to be in the focal point of research due to the importance of transient response in the everyday operating conditions of engines. The majority of studies have focused so far on thermodynamics, as this directly affects heat release predictions and consequently performance and pollutants emissions. On the other hand, issues concerning the dynamics of engine operation are often disregarded or over-simplified. In the present work, an experimentally validated diesel engine simulation code is used to study and evaluate the importance of a notable engine dynamic issue, i.e. the crankshaft torsional (angular) deformations during turbocharged diesel engine operation owing to the difference between instantaneous engine and load (resistance) torques. The analysis aims ultimately in studying the phenomena under the very demanding, and often critical, transient operating conditions. Detailed crankshaft angular momentum equilibrium is formulated that takes into account instantaneous gas, inertia, friction, load as well as stiffness, and damping torque contributions. Details are provided concerning the underlying mechanism of the crankshaft torsional deformations during steady-state and transient operation. This deformation can assume significant values depending on the engine-load configuration (load change, crankshaft stiffness, kind of aspiration of the engine), and as such it is of great importance for safe engine operation.

Keywords: diesel engine, crankshaft, torsional deformation, transient operation

1 INTRODUCTION

The turbocharged diesel engine is nowadays the most preferred prime mover in medium and medium-large units applications (truck driving, land traction, ship propulsion, electrical generation). Moreover, it continuously increases its share in the highly competitive automotive market, owing to its reliability that is combined with excellent fuel efficiency. Particularly, its transient operation is of paramount importance in the everyday operating conditions of engines, being often linked with offdesign (e.g. turbocharger lag) and, consequently, non-optimum performance and increased exhaust emissions.

During the last decades, mathematical simulation has paved the way for an in-depth study of diesel engine processes under both steady-state and transient conditions [**1**–**7**]. However, the majority of research has focused so far on thermodynamics, as this directly affects heat release predictions and consequently performance and pollutants emissions. On the other hand, issues concerning engine dynamics, e.g. connecting rod complex movement, kinematics of the slider-crank mechanism, crankshaft deformations, torsional vibrations etc., are often disregarded or over-simplified, possibly for the sake of speeding up thermodynamic simulation program execution time [**7**].

**Corresponding author: Internal Combustion Engines Laboratory, Department of Thermal Engineering, School of Mechanical Engineering, National Technical University of Athens, 9 Heroon Polytechniou Street, Zografou Campus 15780, Athens, Greece. email: cdrakops@central.ntua.gr*

An important aspect of internal combustion engine operation is that instantaneous engine torque fluctuates significantly during an engine cycle, even under steady-state conditions. The main mechanism behind this is the cyclic nature of gas pressures and inertia reciprocating forces [**8**]. This fluctuation may be of considerable magnitude, particularly during turbocharged diesel engine operation, where the cylinder pressures assume very high values. On the other hand, resistance (load) torque remains practically constant during a cycle, owing to the adequately low non-uniformity of rotation; the latter being, mainly, determined by the flywheel mass moment of inertia (as will be shown in section 2.4 load torque depends mainly on engine speed). As a result, a significant fluctuation occurs in the instantaneous net (engine minus load) torque that eventually leads to cyclic speed irregularities, twists between individual cranks of a multi-cylinder engine and, finally, torsional (angular) deformation of the whole elastic crankshaft. Particularly in modern automotive engines, the above phenomenon is intensified by the flexibility of light-weight crankshafts that may even lead to 'engine roughness' [**9**, **10**]. The crankshaft deformation is further enhanced during transient operation, owing to the dynamic instability induced by the considerable deficit of torque, during the early cycles of the transient event after the new, increased, load or fuelling has been applied.

The instantaneous values of crankshaft torsional deformation should be maintained overall low, in order to avoid excessive stress on the crankshaft and its bearings so that safe engine operation is ensured. In order to be able to study and quantify this deformation, a first satisfactory approach lies in the formulation of detailed crankshaft angular momentum equilibrium. Apart from the well known gas, inertia and load terms, this equilibrium must take into account the *instantaneous* values of all torque contributors, including stiffness, damping, and (engine) friction. A further significant contribution comes from the whirl of engine bearings, which is usually accounted for in multi-body dynamic studies; the latter are based on Lagrangian dynamics and, typically, comprise all rigid body inertia members, support bearings, joints, couplers, and other connections between the various engine components, as well as means of vibration damping [**11**, **12**].

Past research on steady-state engine dynamics can prove useful in describing the detailed crankshaft angular momentum balance needed for torsional deformation studies [**13**–**16**]. However, in all these works the object was the estimation of indicated torque using, for example, sliding mode observers [**13**], or the reconstruction of cylinder pressures from crankshaft angular velocity measurements [**14**, **15**], e.g. for diagnosis purposes [**16**], rather than the investigation of the *instantaneous* crankshaft torsional deformation itself. On the other hand, classic torsional vibration handbooks deal with the subject on a cycle rather than degree crank angle (°CA) basis, for the special, but very important, case where the engine operates at resonance with some harmonic order of the exciting engine forces [**17**, **18**].

As regards the very demanding transient diesel engine operation no data are available, since in all previous simulations the crankshaft has been assumed sufficiently short and rigid. Consequently, no address was made for crankshaft torsional deformation effects [**7**].

In this work, the crankshaft angular momentum equilibrium analysis is expanded and the instantaneous torsional deformation during steady-state and, ultimately, transient conditions are quantified. It is, therefore, believed that useful information will be drawn regarding the underlying thermodynamic-dynamic mechanisms. In order to fulfil this goal, an experimentally validated diesel engine simulation code that follows the filling and emptying approach will be used; this incorporates some important features to account for the peculiarities of transient operation. Improved relations concerning fuel injection, combustion, dynamic analysis, heat transfer to the cylinder walls, friction and multi-cylinder engine operation during transients have been developed, which contribute to an in-depth modelling [**7**, **19**, **20**]. Special care is paid to the formulation of the crankshaft torque balance by taking into account, among other things, the *instantaneous* engine friction torque, using a recently developed detailed friction model, as well as the *instantaneous* gas torque contribution separately from each cylinder when studying the transient operation of a multi-cylinder engine.

Owing to the narrow speed range of the engine in hand, mainly load increases under constant governor setting will be investigated, which, nonetheless, play a significant role in the European or American transient cycles of heavy duty vehicles. Fundamental aspects of crankshaft torsional deformation will be pursued with relation to the initiating in-cylinder pressure and gas torque build-up. A sensitivity analysis will also be carried out in order to establish whether by incorporating a detailed crankshaft submodel, this leads in more accurate predictions of transient engine speed response.

2 SIMULATION ANALYSIS

The block diagram of the simulation model developed is illustrated in Fig. 1, referring to both

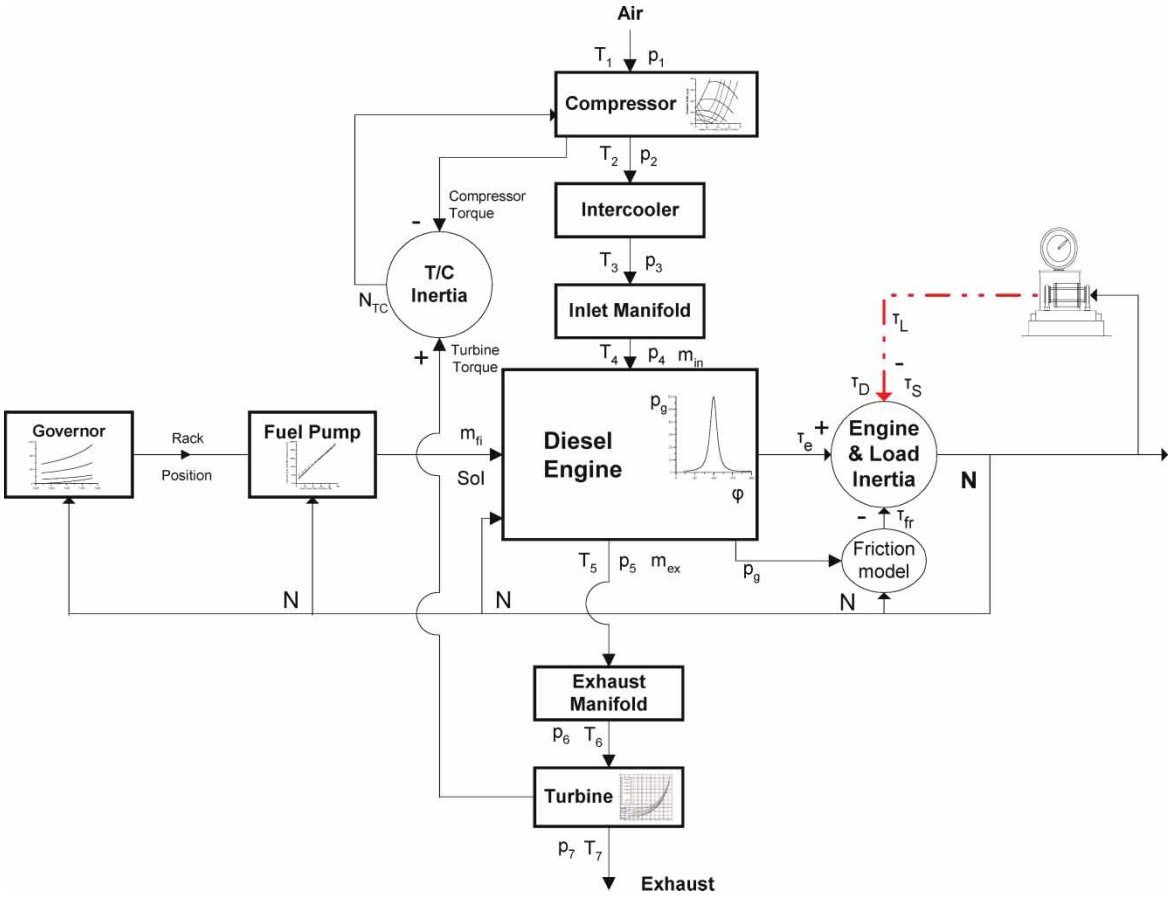

Fig. 1 Block diagram of developed simulation code

steady-state and transient turbocharged diesel engine operation. A brief description of the equations involved will be presented in the next subsections.

2.1 General process description

The present analysis does not, at the moment, include predictions of exhaust gas emissions and, on the other hand, deals with transient operation calculations on a °CA basis. Therefore, a single-zone model following the filling and emptying approach is used for the thermodynamic processes evaluation. This approach is believed to be the best compromise between accuracy and limited PC program execution time [**7**]. The fuel is dodecane ($C_{12}H_{26}$) with a lower heating value, LHV = 42 500 kJ/kg. Perfect gas behaviour is assumed. Polynomial expressions are used for the species considered, concerning the evaluation of internal energy and specific heat capacities for first-law applications to the engine cylinder contents [**3**]. The species considered are O_2, N_2, CO_2, H_2O, and CO; the latter is taken into account, using the corresponding chemical equilibrium scheme, only when the mixture is rich and for gas temperatures exceeding 1400 K, as for example during the early cycles of the transient event where the turbocharger lag is prominent [**7**].

For heat release rate predictions, the fundamental model proposed by Whitehouse and Way [**21**] is used. Especially during transients, the constant K in the (dominant) preparation rate equation of the model is correlated with the Sauter mean diameter (SMD) of the fuel droplets, through a formula of the type $K \propto (1/\mathrm{SMD})^{2.5}$ [**1**].

The improved model of Annand and Ma [**22**] is used to simulate heat loss Q_L to the cylinder walls

$$\frac{\mathrm{d}Q_L}{\mathrm{d}t} = A\left\{\frac{k_g}{D}Re^b\left[a(T_g - T_w) + \frac{a'}{\omega}\frac{\mathrm{d}T_g}{\mathrm{d}t}\right] + c(T_g^4 - T_w^4)\right\} \quad (1)$$

where a, a', b, and c are constants evaluated after experimental matching at steady-state conditions. Further, $A = 2A_{\mathrm{pist}} + A'$, with $A_{\mathrm{pist}} = (\pi D^2/4)$ the piston cross-section area, and $A' = \pi D x$ with x the instantaneous cylinder height in contact with the gas (see equation (2) below). k_g is the gas thermal conductivity, while the Reynolds number Re is calculated with a characteristic speed derived from a k–ε

turbulence model and a characteristic length equal to the piston diameter. During transient operation, the thermal inertia of the cylinder wall is taken into account, using a detailed heat transfer scheme that models the temperature distribution from the gas to the cylinder wall up to the coolant.

2.2 Dynamics of the slider-crank mechanism – detailed connecting rod modelling

At each instant of time, the displacement of the piston from the top dead centre (TDC) is given by [**3**]

$$x(\varphi) = r(1 - \cos\ \varphi) + L_{\text{rod}}\left(1 - \sqrt{1 - \lambda^2 \sin^2 \varphi}\right) \quad (2)$$

where r is the crank radius, $\lambda = r/L_{\text{rod}}$ with L_{rod} the connecting rod length (see also Fig. 2), and the crank angle φ is measured from the TDC position.

Differentiation of the above equation with respect to time, gives the instantaneous piston velocity

$$u_{\text{pist}}(\varphi) = \omega \cdot r \sin \varphi\left(1 + \frac{\lambda \cos\ \varphi}{\sqrt{1 - \lambda^2 \sin^2 \varphi}}\right) \quad (3)$$

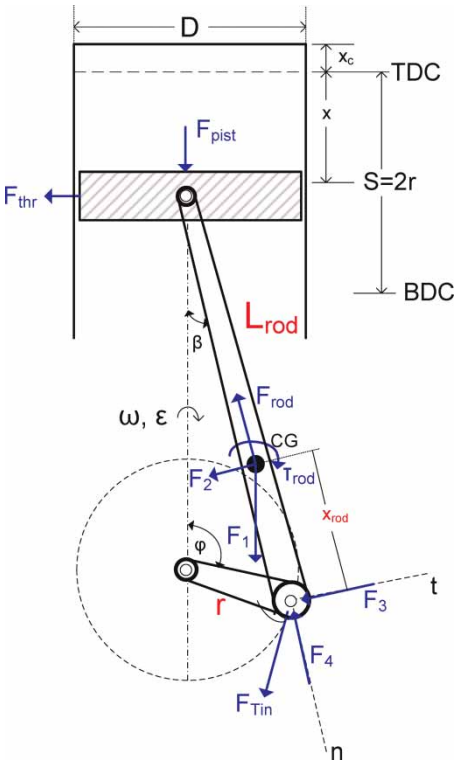

Fig. 2 Slider crank mechanism illustrating forces and torques for the computation of the total inertia force

and by differentiating once again with respect to time, the instantaneous piston acceleration is yielded

$$b(\varphi) = \omega^2 r\left(\cos \varphi + \lambda \frac{\cos 2\varphi + \lambda^2 \sin^4 \varphi}{(1 - \lambda^2 \sin^2 \varphi)^{3/2}} + \frac{1}{\omega^2} \varepsilon \frac{u_{\text{pist}}}{r\omega}\right) \quad (4)$$

The last term on the right hand side of equation (4) takes into account the influence of the crank's angular acceleration, $\varepsilon = \mathrm{d}\omega/\mathrm{d}t$ on the piston linear acceleration.

The connecting rod is usually modelled in the literature as equivalent to two-lumped masses concentrated at its ends, i.e. one reciprocating with the piston assembly and the other rotating with the crank pin. This approach is widely adopted for simplicity reasons. However, it induces errors in the slider-crank mechanism dynamics by miscalculating the actual rod's moment of inertia and the various forces of the kinematic mechanism. For a more accurate computation of engine (inertia) torque, a detailed model of the connecting rod has been developed based on rigid body dynamics [**23**]. Here, the complex, elliptical movement of the rod's centre of gravity that is produced by its reciprocating and rotating motion is analysed.

For the connecting rod angle β, it holds (see also Fig. 2)

$$L \sin \beta = r \sin \varphi \Longrightarrow L \frac{\mathrm{d}\beta}{\mathrm{d}t} \cos\ \beta = r \frac{\mathrm{d}\varphi}{\mathrm{d}t} \cos \varphi \quad (5)$$

Solution of the above equation with respect to $\mathrm{d}\beta/\mathrm{d}t$, yields

$$\frac{\mathrm{d}\beta}{\mathrm{d}t} = \omega_{\text{rod}} = \lambda\omega \frac{\cos\ \varphi}{\cos\ \beta} = \lambda\omega \frac{\cos\ \varphi}{(1 - \lambda^2 \sin^2\ \varphi)^{1/2}} \quad (6)$$

Differentiation of the previous equation with respect to time, gives

$$\frac{\mathrm{d}^2\beta}{\mathrm{d}t^2} = \frac{\mathrm{d}\omega_{\text{rod}}}{\mathrm{d}t} = \varepsilon_{\text{rod}} = \lambda\omega^2 \sin\ \varphi \frac{\lambda^2 - 1}{(1 - \lambda^2 \sin^2\ \varphi)^{3/2}} + \lambda\varepsilon \frac{\cos\ \varphi}{(1 - \lambda^2 \sin^2\ \varphi)^{1/2}} \quad (7)$$

In the above relations, ω_{rod} and ε_{rod} are the angular velocity and acceleration of the connecting rod's centre of gravity, respectively.

With reference to Fig. 2(a) (moving) frame of reference of orthogonal axes (n, t) is considered, which is fixed on the rod, with directions parallel and perpendicular to the rod's axis, respectively; they have

components F_4 and F_3 of the crankpin force on them, respectively.

A balance of all forces acting on the connecting rod, analysed in n and t directions, gives

n-axis forces

$$F_4 + F_{\text{pist}} \cos\beta + F_{\text{thr}} \sin\beta = F_{\text{rod}} - F_1 \cos\beta \tag{8}$$

t-axis forces

$$F_3 - F_{\text{pist}} \sin\beta + F_{\text{thr}} \cos\beta = F_2 + F_1 \sin\beta \tag{9}$$

A balance of torques with respect to the crankpin axis, gives

$$\begin{aligned} &- F_{\text{thr}} \cdot (L_{\text{rod}} \cos\beta) + F_{\text{pist}} \cdot (r \sin\varphi) \\ &\quad = G_{\text{rod}} \cdot \varepsilon_{\text{rod}} - F_1 \cdot (x_{\text{rod}} \sin\beta) - F_2 x_{\text{rod}} \end{aligned} \tag{10}$$

In the above equations, torque $\tau_{\text{rod}} = G_{\text{rod}}\varepsilon_{\text{rod}}$ with G_{rod} the connecting rod's real mass moment of inertia with respect to its centre of gravity, $F_{\text{pist}} = -m_{\text{pist}}b$ is the longitudinal force along the cylinder axis acting on the piston assembly to produce its acceleration [**8**] (piston acceleration $b(\varphi)$ has been defined in equation (4)), and $F_1 = -m_{\text{rod}}b$ is the force acting on the connecting rod centre of gravity due to the linear acceleration of the piston. Also, $F_2 = m_{\text{rod}}(L - x_{\text{rod}})\varepsilon_{\text{rod}}$ and $F_{\text{rod}} = m_{\text{rod}}(L - x_{\text{rod}})\omega_{\text{rod}}^2$, with $(L - x_{\text{rod}})\varepsilon_{\text{rod}}$ the tangential component and $(L - x_{\text{rod}})\omega_{\text{rod}}^2$ the normal component of the rod's centre of gravity acceleration with respect to the piston pin.

The system of equations (8) to (10) can be solved for the unknown forces F_{thr}, F_3, and F_4. Force F_{thr} is the inertia component of the thrust force acting by the piston on the side wall of the cylinder. The sum of the projections of forces F_3 and F_4 on an axis perpendicular to the crank radius produces the tangential (inertia) force F_{Tin}, due to the inertia of the moving parts (piston assembly and connecting rod) acting on the crank, that is

$$F_{\text{Tin}} = F_3 \cos(\varphi + \beta) + F_4 \sin(\varphi + \beta) \tag{11}$$

The latter will be used in section 2.4 for the computation of the engine indicated torque.

2.3 Friction

For the calculation of friction inside the cylinder, the model proposed by Taraza *et al.* [**24**] is adopted. It describes the non-steady profile of friction torque during each cycle, based on fundamental friction analysis. Here, the total amount of friction is divided into four parts, i.e. piston rings assembly, loaded bearings, valve train, and auxiliaries. Total friction torque, T_{fr}, at each °CA is the sum of the above terms. The important outcome here is that this friction torque varies during the engine cycle, especially around 'hot' TDC, unlike the usually applied 'mean' f.m.e.p. equations where friction torque remains constant throughout each cycle [**7**].

It should be mentioned at this point, that the particular model is a generic friction model that was developed using simplified equations of the various principal friction components. More detailed, analytical methods are available in the literature, especially for the cases of piston rings and piston skirt, both of which suffer mixed regime of lubrication around top and bottom dead centres [**25**].

2.4 Crankshaft torque equilibrium

The crankshaft is considered as a flexible, elastic body that may deform during engine operation; it is simulated using the lumped mass model of Fig. 3. A condensed crankshaft model was chosen, i.e. rigid enough between the cylinders and elastic between flywheel and load. The elastic crankshaft rotary motion is excited by the gas and inertia torque fluctuation. The following two, non-linear differential equations apply [**7**, **13**, **26**]

$$T_{\text{e}}(\varphi) - T_{\text{fr}}(\varphi) - T_{\text{S}} - T_{\text{D}} = (G_{\text{e}} + G_{\text{fl}} + G_{\text{coupl}})\frac{\text{d}\omega}{\text{d}t} \tag{12a}$$

$$\tau_{\text{S}} + \tau_{\text{D}} - \tau_{\text{L}}(\varphi_L) = G_{\text{L}}\frac{\text{d}\omega_{\text{L}}}{\text{d}t} \tag{12b}$$

Here, G_{e}, G_{fl}, G_{coupl}, and G_{L} are the engine, flywheel, elastic coupling, and load mass moments of inertia, respectively (considered constant, although, in the general case, the engine moment of inertia may vary with crank angle [**27**]*), $\omega = \text{d}\varphi/\text{d}t$ is the engine angular velocity, $\omega_{\text{L}} = \text{d}\varphi_{\text{L}}/\text{d}t$ is the load angular velocity, and the torsional deformation of the crankshaft due to the torque difference between engine and load is defined as $\varphi - \varphi_{\text{L}}$. Also, T_{e} denotes the engine indicated torque that includes gas, inertia and (the negligible) gravitational forces contributions. Engine torque is mostly dependent on

** For the present engine-load configuration, the total mass moment of inertia is very high due to the dominant contribution of the flywheel (see data in Table 1), so that the differentiation of (engine) mass moment of inertia with crank angle is neglected in the two lumped-mass model considered in Fig. 3. Nonetheless, for the analysis of Fig. 8 in section 4, where the angular deformation between cylinders 3 and 4 will be studied, the variation of cylinder moment of inertia with crank angle has been taken into account.*

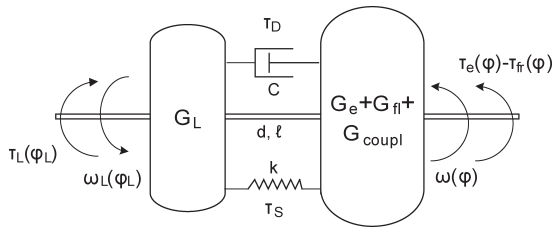

Fig. 3 Schematic arrangement of the engine-load dynamic system for the crankshaft angular momentum equilibrium analysis

accurate combustion modelling and is given explicitly by

$$\begin{aligned} T_{\mathrm{e}}(\varphi) &= T_{\mathrm{g}}(\varphi) + T_{\mathrm{in}}(\varphi) + T_{\mathrm{gr}}(\varphi) \\ &= \left[\left(p_{\mathrm{g}}(\varphi) \cdot A_{\mathrm{pist}} \cdot \frac{u_{\mathrm{pist}}(\varphi)}{r\omega}\right) + F_{\mathrm{Tin}}(\varphi) \right. \\ &\quad \left. + \left(m_{\mathrm{l}} \mathrm{g} \frac{u_{\mathrm{pist}}(\varphi)}{r\omega} + m_{\mathrm{r}} \mathrm{g} \sin\,\varphi \right) \right] \cdot r \end{aligned} \tag{13}$$

In the above relation, $p_{\mathrm{g}}(\varphi)$ is the instantaneous cylinder pressure, $m_{\mathrm{l}} = m_{\mathrm{pist}} + m_{\mathrm{rod.l}}$ is the reciprocating mass, $m_{\mathrm{r}} = m_{\mathrm{crank}} + m_{\mathrm{rod.r}}$ is the rotating mass, and F_{Tin} is the torsional inertia force calculated from equation (11).

For the torsional stiffness and damping torques it holds, respectively,

$$T_{\mathrm{S}} = k(\varphi - \varphi_{\mathrm{L}}) \tag{14a}$$

$$T_{\mathrm{D}} = C(\omega - \omega_{\mathrm{L}}) \tag{14b}$$

with k the stiffness coefficient, which is given by

$$k = \frac{\Theta \cdot J_{\mathrm{P}}}{\ell} = \frac{\Theta}{\ell} \cdot \frac{\pi d^4}{32} \tag{15}$$

and C the damping coefficient, which is defined by the characteristics of the (viscous or rubber) damper mounted on the engine's crankshaft. In equation (15), Θ is the shear modulus (in $\mathrm{N/m^2}$), J_{P} is the polar moment of inertia (in $\mathrm{m^4}$) of the shaft cross section and d, ℓ are the shaft diameter and length, respectively, between engine flywheel and load. Both coefficients are assumed constant through the analysis.

It is reminded here that if the crankshaft is assumed short and rigid enough (as for the usual case in transient simulations), $\varphi \equiv \varphi_{\mathrm{L}}$. Thus, by adding both sides of equations (12a) and (12b), these are replaced by the simple equation: $T_{\mathrm{e}}(\varphi) - T_{\mathrm{fr}}(\varphi) - T_{\mathrm{L}}(\varphi) = G_{\mathrm{tot}}(\mathrm{d}\omega/\mathrm{d}t)$, where G_{tot} represents the total mass moment of inertia of the engine-load configuration reduced to the crankshaft axis.

Finally, T_{L} is the load torque, which is approximated by the following relation

$$T_{\mathrm{L}}(\varphi_{\mathrm{L}}) = \mathrm{C}_1 + \mathrm{C}_2 \omega_{\mathrm{L}}^{\mathrm{C}_3} \tag{16}$$

For a linear load-type (i.e. electric brake, generator) $\mathrm{C}_3 = 1$, while for a quadratic load-type (i.e. hydraulic brake, fixed pitch propeller, vehicle aerodynamic resistance) $\mathrm{C}_3 = 2$, with C_1 the speed-independent load term (e.g. road slope).

The differential equations (12a) and (12b) are solved at each °CA, using the instantaneous torque terms from all six cylinders of the present engine. Particularly, as regards the gas torque during transients, the individual cylinder gas pressures derive from the thermodynamic model, with application of the 'true multi-cylinder' approach described later in subsection 2.6. Solution of equations (12) provides, at each °CA, the individual engine-side and load-side rotational speeds ω and ω_{L} as well as the respective angles φ and φ_{L} and, hence, the torsional deformation $\varphi - \varphi_{\mathrm{L}}$.

Previous researchers [**14**, **16**] have described an even more detailed angular momentum balance, by taking into account all possible crankshaft deformations between pulley, each cylinder of a multi-cylinder diesel engine, and flywheel. This eventually led to a system of 6–10 differential equations, depending on the number of cylinders of the engine in hand. They also preferred solution of the respective differential equations using Fourier analysis of the gas and inertia torque harmonics. This approach is not, however, suitable for transient operation cases, which forms the main goal of investigation in the present work.

2.5 Fuel pump operation

Instead of applying the steady-state fuel pump curves during transients, a fuel injection model, experimentally validated at steady-state conditions, is used. Thus, simulation of the fuel pump-injector lift mechanism is accomplished, taking into account the delivery valve and injector needle motion [**28**]. The unsteady gas flow equations are solved using the method of characteristics, providing the dynamic injection timing as well as the duration and the rate of injection for each cylinder at each transient cycle. The obvious advantage here is that the *transient* operation of the fuel pump is also taken into account. This is mainly accomplished through the fuel pump residual pressure value, which is built up together with the other variables during the transient event.

2.6 Multi-cylinder engine modelling

At steady-state operation, the performance of each cylinder is essentially the same, due to the

quasi-steady position of the governor clutch resulting in the same amount of fuel being injected per cycle, and the quasi-steady turbocharger compressor operating point. Under transient operation, however, each cylinder experiences *different* fuelings and air mass flowrates during the same engine cycle. This happens due to the combined effect of: (a) the continuous movement of the fuel pump rack that is initiated by a load or speed change, and (b) the continuous movement of the turbocharger compressor operating point. As regards speed changes, only the first cycles are practically affected. However, when load changes are investigated, significant variations can be experienced throughout the whole transient cycle. The usual approach, here, is the solution of the governing equations for one cylinder and the subsequent use of suitable phasing images of this cylinder's behaviour. This approach is widely popular for limiting the computational time [**7**]. Unlike this, the present research group has developed a true 'multi-cylinder' engine model. Here, all the governing differential and algebraic equations are solved individually for every one cylinder of the six-cylinder engine under study, according to the current values of the fuel pump rack position and turbocharger compressor flow. This results in (significant) differentiations in both fuelling and air mass flowrates for each cylinder during the *same* cycle of a transient event, affecting, among other things, the crankshaft torsional deformation results.

3 EXPERIMENTAL VALIDATION

The objective of the experimental test bed developed was to investigate the steady-state and transient performance of the engine in hand. To accomplish this task the engine was coupled to a hydraulic brake (dynamometer). Strategic measuring points were connected to a computer data logging system for recording and processing engine and turbocharger variables. The experimental facilities can be divided into two parts: (a) the engine test bed, and (b) the data logging and processing system. The basic data for the engine and turbocharger are given in Table 1. A schematic arrangement of the test bed instrumentation is illustrated in Fig. 4.

Table 1 Basic data for engine and turbocharger

	MWM TbRHS 518S
Engine Model and Type	In-line, six-cylinder, four-stroke, compression ignition, turbocharged, aftercooled, heavy-duty
Speed range	1000/1500 r/min
Bore/stroke	140/180 mm
Compression ratio	17.7:1
Maximum power	320 HP (236 kW) @ 1500 r/min
Maximum torque	1520 Nm @ 1250 r/min
Turbocharger	Single-stage, centrifugal compressor, single-stage, twin entry, axial turbine
Moment of inertia	Engine & brake: 15.60 kg m^2 Turbocharger: 7.5×10^{-4} kg m^2
Shaft rigidity	240 000 Nm/rad

3.1 Engine test bed instrumentation

The experimental investigation was conducted on an MWM TbRHS 518S, six-cylinder, turbocharged and aftercooled, medium-high speed diesel engine of marine duty.

Apart from the engine and dynamometer, the main parts of the test installation include:

(a) tank and flow-meter for measuring diesel fuel consumption rate;
(b) turbocharger compressor boost pressure manometer;
(c) compressor inlet and exit thermometers and aftercooler exit air thermometer;
(d) magnetic pick-up TDC marker and r/min indicator;
(e) Kistler piezotron pressure transducer with a voltage amplifier for continuously measuring the turbocharger compressor boost pressure;
(f) Kistler piezoelectric transducer with voltage amplifier for continuously measuring the cylinder pressure diagram;
(g) Bosch RTT-100 smokemeter fitted into the exhaust pipe downstream of the turbine;
(h) Schaevitz–Lucas linear variable displacement transducer (LVDT) for continuously measuring the fuel pump rack position;
(i) AEG stroboscope for the measurement of (steady-state) turbocharger speed;
(j) J and K type thermocouples for measuring the temperatures of the exhaust gas after each cylinder and downstream of the turbine;
(k) Tektronix storage oscilloscope.

The data acquisition and processing system for the engine test bed comprised:

(a) a Metrabyte DASH-16F, high-speed data acquisition card for measuring pressures, LVDT and TDC signals;
(b) an Advantech PCL-818HD, high-speed data acquisition card with PCLD-789D expansion card for various temperature measurements;
(c) two IBM compatible PCs, properly interfaced for fast data acquisition and recording, on the buses of which the two cards mentioned above were mounted.

Both sampling systems use a fast 12-bit converter with an 8 μs analogue-to-digital conversion time,

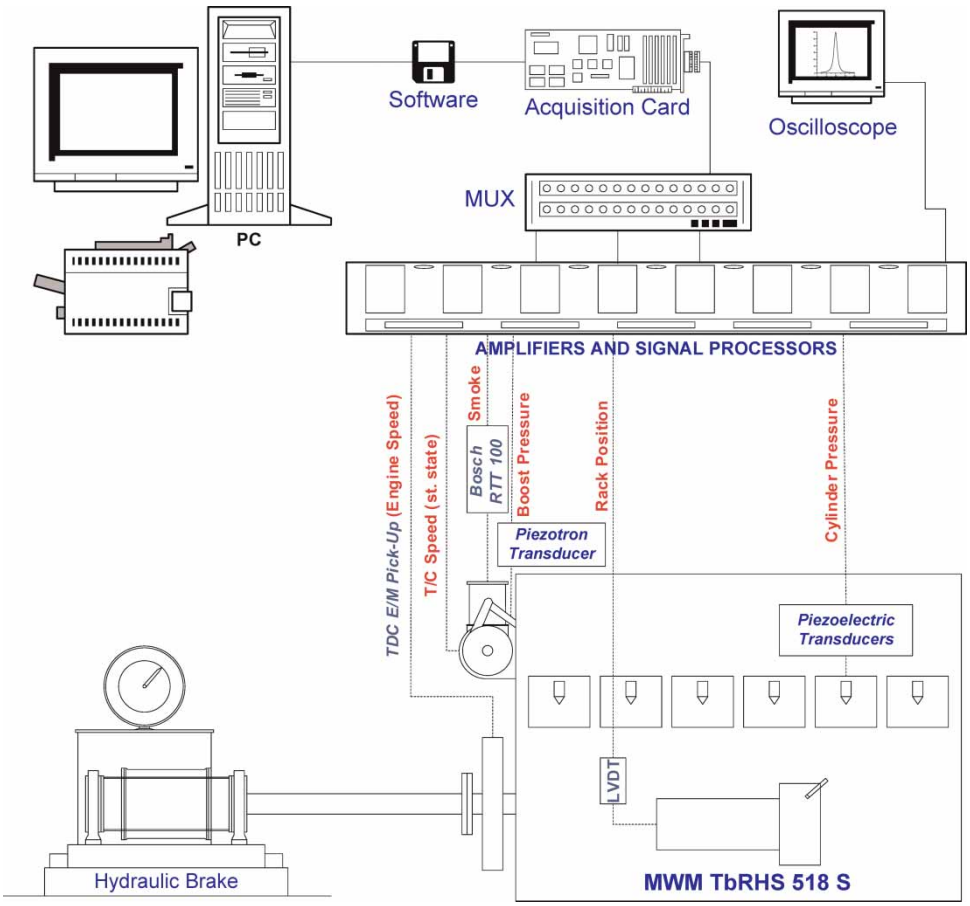

Fig. 4 Schematic arrangement of engine test bed instrumentation

giving a maximum throughput rate of 100 kHz in direct memory access mode.

3.2 Experimental results

The first requirement from the engine test bed instrumentation was to investigate the steady-state performance of the engine in hand. For this purpose, an extended series of steady-state trials was conducted in order on the one hand to examine the model's predictive capabilities and, on the other, to calibrate successfully the individual submodels described in the previous sections. By so doing, the constants for the combustion, heat transfer, friction, etc., submodels were made possible to be estimated. The investigation of transient operation was the next task. Since the particular engine is one with a relatively small speed range, mainly load changes (increases) with constant governor setting were examined [**19**]. A typical example of a conducted transient experiment is given in Fig. 5. Here, the initial load was 10 per cent of the full engine load at 1180 r/min. The final applied load was almost 50 per cent of the full engine load. The non-linear character of the load application, which could not be accounted for in the simulation, is responsible for the differences observed in boost pressure and engine speed response. The particular hydraulic brake has a very high mass moment of inertia, of the order of 5.375 kg m^2, resulting in long, abrupt and non-linear actual load-change profiles. Nonetheless, the matching between experimental and predicted transient responses seems satisfactory for all engine and turbocharger variables measured (engine speed, fuel pump rack position, and boost pressure); it is believed to form a sound basis for the theoretical investigation that follows.

4 RESULTS AND DISCUSSION

Figure 6 illustrates the development of crankshaft torsional deformation, i.e. term $(\varphi - \varphi_L)$ from equations (12), during typical, steady-state, diesel engine operation. A 'single-cylinder version' of the current engine is initially chosen for the analysis, in order for the results to be directly comparable to the in-cycle pressure and torque build-up. The data presented in Fig. 6 are in accordance with the findings of previous works at steady-state conditions [**16**, **29**], as regards both in-cycle profile and absolute values.

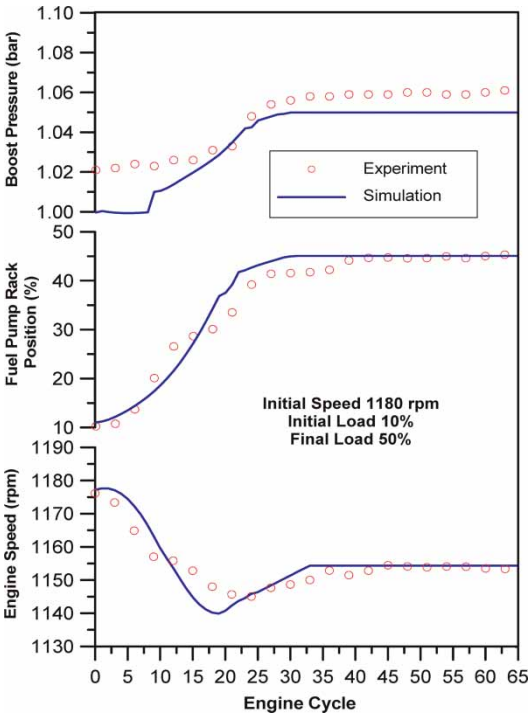

Fig. 5 Experimental and predicted engine transient response to an increase in load

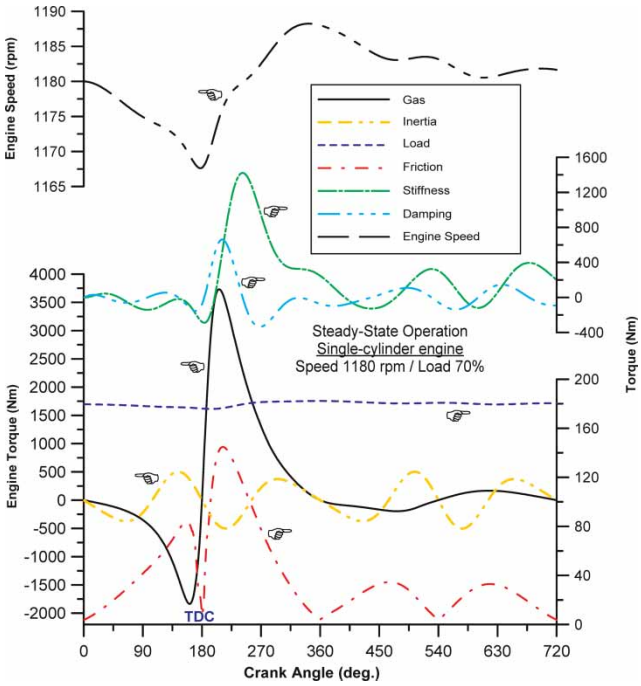

Fig. 7 Engine speed and various torque contributors build-up during steady-state, single-cylinder engine operation

Figure 6 should be studied in conjunction with Fig. 7 that depicts the development of all torque contributors during the same engine cycle.

During compression (0–180°CA), a deficit of gas torque exists that leads to engine speed decrease (upper subdiagram of Fig. 7) and to the 'negative' crankshaft deformation shown in Fig. 6; torque, speed, and deformation all peak around 'hot' TDC. After the start of combustion, there is a surplus of torque, as now the engine enters the power producing phase of operation. Consequently, 'positive' deformation is established, while the instantaneous engine speed increases. This lasts for the whole expansion stroke. The considerably higher amount of engine torque produced during expansion leads to the greater local peak in crankshaft deformation, i.e. 0.16° occurring at about 55 °CA after 'hot' TDC, compared to the local minimum of −0.03° at 180 °CA (70 per cent load operation).

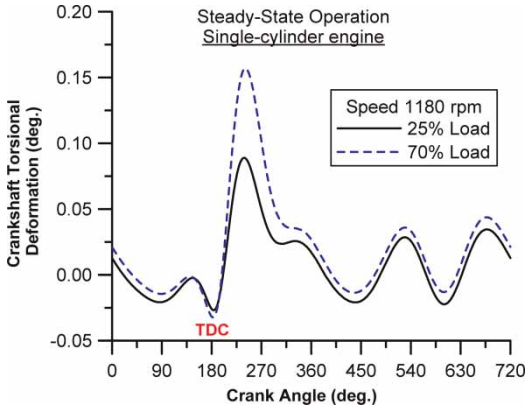

Fig. 6 Development of the crankshaft torsional deformation during steady-state, single-cylinder engine operation for two different loads

The main mechanism behind the crankshaft torsional deformation profile, over an engine cycle, is clearly the gas torque because of its direct impact on the total engine torque. This confirms the results of Chen and Chen [**16**], who concluded that torsional angle amplitude is, practically, a linear function of the corresponding gas torque. Closer examination of Fig. 6 reveals that inertia torque influence is also present, mainly during the open part of the cycle where the cylinder pressure is low, as well as during the second half of compression. For the present engine the inertia contribution is rather small, due to the low engine speed (recall that inertia forces vary as the square of the engine speed). Crankshaft torsional deformation may assume again negative values during the open part of the cycle, due to the inertia torque effects.

Of significant importance is the variation of friction torque over the engine cycle. The usual approach, when studying engine friction, is the use of 'mean' f.m.e.p. relations. This is not the case, however, in this work, as application of the detailed Taraza *et al.* [**24**] friction model assisted in establishing the real

friction profile during the engine cycle. Notice, in Fig. 7, the increased values for a period of almost 180 degrees CA around 'hot' TDC. These differentiate the deformation results obtained, compared to the case where friction would have been computed by the 'mean' f.m.e.p. relations.

Another interesting finding is that stiffness and damping instantaneous torques may reach high values during an engine cycle. The profile of stiffness torque follows the torsional deformation as dictated by equation (14a). The profile of damping torque is indicative of the instantaneous difference between engine and load speeds ($\omega - \omega_L$). Owing to the 'internal inertia' of these 'processes', the respective torque peaks observed in the centre subdiagram of Fig. 7 may be delayed compared to the initiating gas torque or cylinder pressure. However, despite their relatively high instantaneous values, both stiffness and damping torques' mean (over the engine cycle) values are negligible compared to the gas or load torque. As a result, the usually applied assumption is justified, i.e. of neglecting these torques for the calculation of *mean* engine speed.

The torsional deformation for the 25 per cent load is also depicted in Fig. 6 for comparison purposes. Here, lower maxima of crankshaft deformation are, overall, observed. This was intuitively expected, because of the lower values of fuelling and consequently engine gas torque produced during this cycle (inertia forces retain the same values as in the 70 per cent load case, since the engine speed is the same). Similarly, smaller deformations are to be expected for naturally aspirated diesel or for spark ignition (Otto) engines, where the cylinder pressures are much lower. In the latter cases, a greater influence of inertia torque is also expected, particularly for the small Otto (car) engines operating at high rotational speeds.

The main findings of the 'single-cylinder' configuration can be extended to the (real) multi-cylinder engine operation, which is depicted in Fig. 8 for the same engine load*. The effect of the number of cylinders is the dominant factor in the multi-cylinder analysis of Fig. 8. Owing to the relatively high load (70 per cent), there is always an adequate surplus of gas torque that prevents the crankshaft torsional deformation from reaching negative values.

An interesting case is illustrated at the lower part of Fig. 8. Here, the operation of cylinders 3 and 4 has been isolated and the torsional deformation of the crankshaft section that is surrounded by these

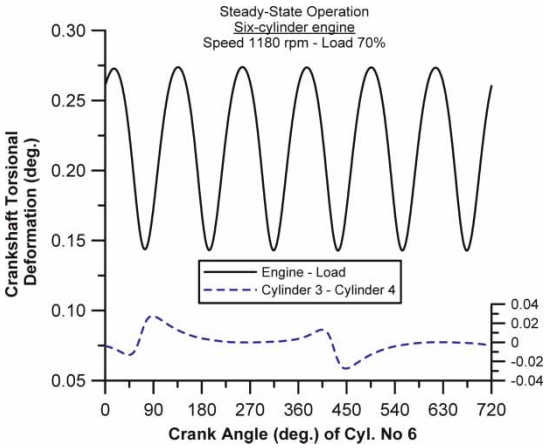

Fig. 8 Development of the crankshaft torsional deformation during steady-state multi-cylinder engine operation

cylinders is studied. Again, the deformation profile closely follows the gas torque development, but now both cylinders' torques are in phase (there is no such thing as 'resistance' torque in this case). The distance between the two peaks observed corresponds to the firing interval between these two cylinders, i.e. 360 °CA. Owing to the much smaller length of the crankshaft axis between cylinders 3 and 4, the stiffness coefficient, k_{34}, is now one order of magnitude higher, thus leading to much smaller deformations during the 70 per cent load operation compared to the engine-load results (upper graph in Fig. 8).

The investigation of the results during transient operation was the next task. When studying the development of crankshaft deformation, it is imperative that instantaneous values for each torque contributor are taken into account. In the present analysis, the dominant gas torque term is computed during transients *separately* for each cylinder, using the multi-cylinder engine model described earlier. Thus, during the same engine cycle, differentiations are observed between the gas torques of individual cylinders due to the continuous movement of the fuel pump rack.

Figure 9 depicts the development of the maximum and the mean, over each engine cycle, deformation and stress for a typical load increase transient of 10–75 per cent commencing from an engine speed of 1180 r/min. The response of the crank angle where the maximum deformation occurs (corresponding to the second of the six 'similar' peaks of the six-cylinder engine under study) is also depicted in the same figure.

Initially, the deformation is negligible due to the low engine load (see Fig. 6). As the governor responds to the drop in engine speed caused by the abrupt load increase, fuelling increases too (right-hand side

* *Since the mass moments of inertia of the 'single' cylinder and the six-cylinder engines' are not proportional, no conclusion is meant to be drawn concerning the instantaneous maxima or minima of the angular deformations observed in Figs 6 and 8.*

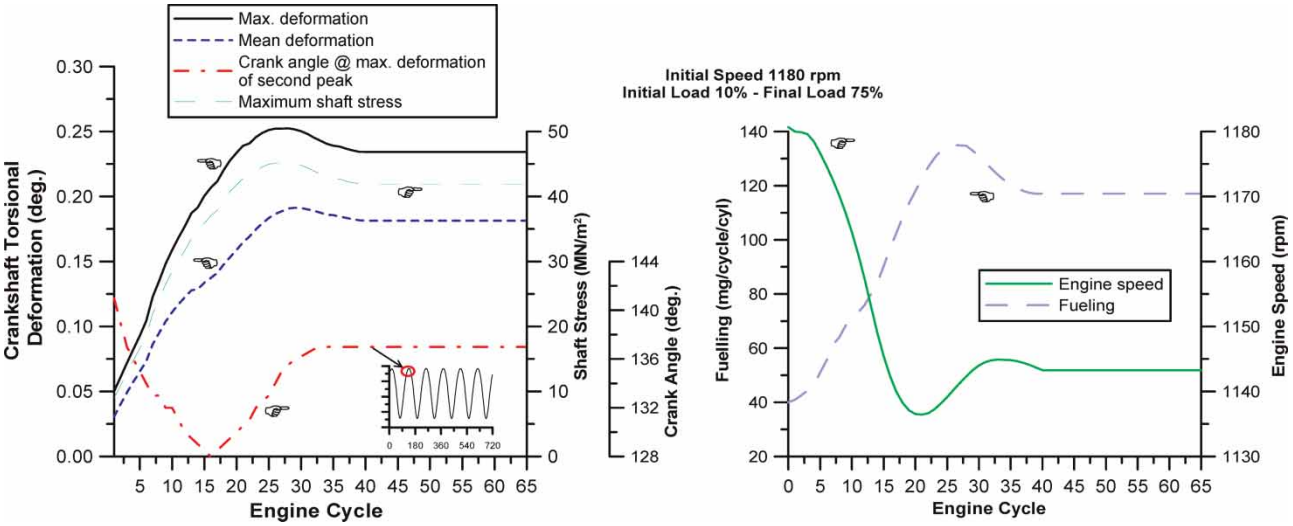

Fig. 9 Development of the maximum and mean, over an engine cycle, crankshaft torsional deformation, and stress during a 10–75 per cent load increase transient event

subdiagram of Fig. 9) leading in higher gas pressures and torques throughout the cycle. This results in greater maximum and mean, over the engine cycle, deformations, as well as in a gradual shift of the crank angle where the peak occurs earlier in the cycle. It is important to note that the instantaneous maximum deformation is considerably higher (up to 50 per cent for the cases examined in this work) than the respective mean value in the same cycle; this justifies the analysis on a °CA basis, in order to be able to estimate the 'true' maximum stress (left subdiagram of Fig. 9) that is instantaneously experienced by the (crank)shaft, that is

$$\sigma_{\max} = \frac{\Theta}{2}\frac{d}{\ell}\Delta\varphi_{\max} = \frac{\Theta}{2}\frac{d}{\ell}(\varphi_{\mathrm{e}} - \varphi_{\mathrm{L}})_{\max} \tag{17}$$

It should be pointed out here that the evolution of transient maximum or mean, over the engine cycle, deformation and, hence, stress develop in a different way compared to the corresponding steady-state engine operation points (i.e. at the same engine speed and fuel pump rack position). The difference is, mainly, attributed to:

(a) the different air-fuel equivalence ratios experienced during transients owing to the turbocharger lag, which significantly affects the air-mass flowrate, particularly during the early cycles of the transient event;
(b) the transient operation of the fuel pump that differentiates from the steady-state fuel pump curves.

The above results are expanded in Fig. 10, by showing the 'wave' of crankshaft deformation build-up for several cycles of the same transient event. It can be further observed that the increase in loading/fuelling leads in greater in-cycle fluctuations of the deformation too (see Fig. 6).

From the analysis it has been revealed that, in principle, the main parameters affecting the profile and values of crankshaft torsional deformations during transients, are the applied engine load and the crankshaft stiffness.

The effect of the magnitude of the applied load is demonstrated in Fig. 11. A higher applied load leads to higher fuelling rates and, thus, cylinder pressures/gas torques. Consequently, after the start of combustion, the surplus of net torque is much higher now resulting in greater peaks of crankshaft deformation (cf. the two load curves in Fig. 6 for steady-state engine operation).

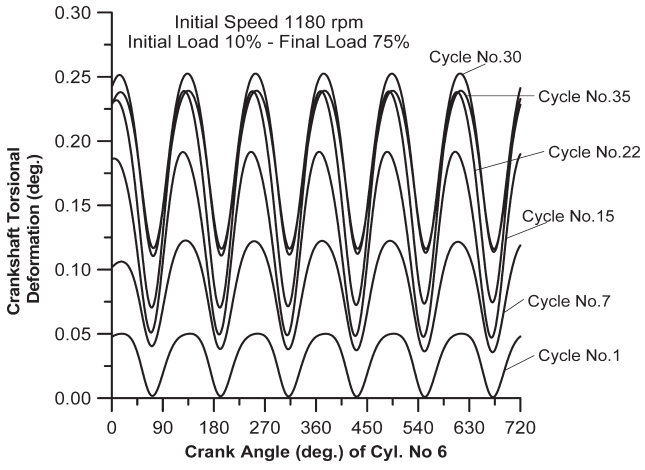

Fig. 10 Development of the crankshaft torsional deformation during various cycles of the 10–75 per cent load increase transient

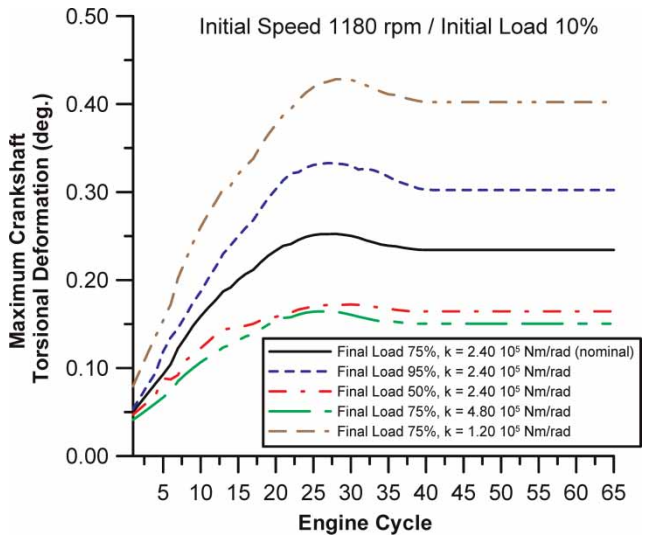

Fig. 11 Effect of the load change magnitude and the crankshaft stiffness on the crankshaft torsional deformation during transient operation after a load increase

The effect of crankshaft stiffness on the torsional deformation is also presented in Fig. 11. As expected, the more rigid the crankshaft (greater values of '*k*' in equation (14a)), the smaller the torsional deformation observed throughout the whole event. An increase of the order of 160 per cent in the deformation peak is observed when comparing the results between the double and the half stiffness coefficient values. Low stiffness (e.g. due to great physical length of the crankshaft) acts, practically, in the same way as the low mass moment of inertia, i.e. it allows higher acceleration rates throughout the cycle, thus, lowering the engine non-uniformity of rotation. In modern automotive engines, the trend of lighter crankshaft configurations may intensify the above-mentioned deformations, leading even to rough engine operation. The above phenomenon has been studied in multi-body dynamics studies [**9**] or by applying a dynamic stiffness matrix method, or transfer matrix method as, for example, in Okamura and Morita [**10**].

Finally, a sensitivity analysis was carried out, which showed that the detailed formulation of the crankshaft angular momentum (equations (12)) does *not* diversify the overall (transient) engine speed response predictions. Hence, its incorporation into a transient simulation code is necessary only if the study of torsional deformation is the object of research, as it is actually the case for this work.

5 CONCLUSIONS – FUTURE WORK

An experimentally validated simulation code developed has been used to study the development of crankshaft torsional deformations during steady-state and transient operation of a turbocharged diesel engine.

When formulating the crankshaft angular momentum equilibrium, care was taken to apply *instantaneous* values for all torque terms, including engine friction (using a detailed model), stiffness and damping, whereas the gas torque contribution was computed separately for each cylinder using a 'real multi-cylinder' engine model.

Application of the detailed crankshaft angular momentum equilibrium helped in quantifying crankshaft torsional deformation values during steady-state and transient operation. Improved understanding of contributing and controlling factors is believed to have been achieved. From the analysis of the present engine-load configuration, the following results were reached.

1. Engine torque was identified as the main contributor in crankshaft deformation profile and peak values. Inertia torque influences the crankshaft deformation mainly during the open part of the cycle (of a single-cylinder engine), but it was overall limited for the present engine due to its, relatively, low speed.
2. Stiffness and damping torques can assume significant instantaneous values during a cycle. However, their mean, over the engine cycle, values are negligible compared to the engine and load terms.
3. Local deformation between individual cylinders is always of much lesser importance, because of the considerably higher stiffness coefficients involved.
4. Mean and maximum, over an engine cycle, deformation response can assume significant values during transient operation, depending on the load increase schedule. The instantaneous maximum deformation can be up to 50 per cent higher compared to the respective mean value in the same transient cycle.
5. The transient deformations develop in a different way compared to the corresponding steady-state operating points, owing to the differentiated fuelling and air-mass flowrates experienced during transients.
6. The assumption of the crankshaft assumed sufficiently rigid is well justified, as regards accuracy of the mean, over the engine cycle, engine speed response predictions during transient operation.
7. Smaller load changes as well as more rigid construction of the crankshaft are identified as key parameters for reducing the crankshaft torsional deformation during transients.

REFERENCES

1 **Benson, R. S.** and **Whitehouse, N. D.** *Internal combustion engines*, 1979 (Pergamon Press, Oxford).
2 **Watson, N.** and **Janota, M. S.** *Turbocharging the internal combustion engine*, 1982 (MacMillan, London).
3 **Heywood, J. B.** *Internal combustion engine fundamentals*, 1988 (McGraw-Hill, New York).
4 **Stone, R.** *Introduction to internal combustion engines*, 3rd edition, 1999 (MacMillan, London).
5 **Watson, N.** Eliminating rating effects on turbocharged diesel engine response. SAE paper 840134, 1984.
6 **Benajes, J., Lujan, J. M., Bermudez, V.,** and **Serrano, J. R.** Modelling of turbocharged diesel engines in transient operation. Part 1: insight into the relevant physical phenomena. *Proc. Instn Mech. Engrs, Part D: J. Automobile Engineering*, 2002, **216**, 431–441.
7 **Rakopoulos, C. D.** and **Giakoumis, E. G.** Review of thermodynamic diesel engine simulations under transient operating conditions. *Trans. SAE, J. Engines*, 2006, **115**, 467–504 (SAE paper 2006-01-0884, 2006).
8 **Taylor, C. F.** *The internal combustion engine in theory and practice*, vol. 2, 1985 (MIT Press, Cambridge, MA).
9 **Kushwaha, M., Gupta, S., Kelly, P.,** and **Rahnejat, H.** Elasto-multi-body dynamics of a multicylinder internal combustion engine. *Proc. Instn Mech. Engrs, Part K: J. Multi-body Dynamics*, 2002, **216**(K4), 281–293.
10 **Okamura, H.** and **Morita, T.** Efficient modelling and analysis for crankshaft three-dimensional vibrations under firing conditions. *Proc. Instn Mech. Engrs, Part K: J. Multi-body Dynamics*, 1999, **213**(K1), 33–44.
11 **Rahnejat, H.** Multi-body dynamics: historical evolution and application. *Proc. Instn Mech. Engrs, Part C: J. Mechanical Engineering Science*, 2000, **214**(C1), 149–173.
12 **Boysal, A.** and **Rahnejat, H.** Torsional vibration analysis of a multi-body single cylinder internal combustion engine model. *Appl. Math. Model.*, 1997, **21**(8), 481–493.
13 **Wang, Y. Y., Krishnaswami, V.,** and **Rizzoni, G.** Event-based estimation of indicated torque for I.C. engines using sliding mode observers. *Control Eng. Pract.*, 1997, **5**(8), 1123–1129.
14 **Taraza, D., Henein, N. A.,** and **Bryzik, W.** Determination of the gas-pressure torque of a multicylinder engine from measurements of the crankshaft's speed variation. SAE paper 980164, 1998.
15 **Zweiri, Y. H., Whidborne, J. F.,** and **Seneviratne, L. D.** Numerical inversion of the dynamic model of a single-cylinder diesel engine. *Commun. Numer. Methods. Eng.*, 2000, **16**, 505–517.
16 **Chen, S. K.** and **Chen, S.** Engine diagnostics by dynamic shaft measurement: a progress report. SAE paper 932412, 1993.
17 **Ker Wilson, W.** *Practical solution of torsional vibration problems*, 3rd edition, 1956–1969 (Chapman and Hall, London).
18 **Haug, K.** *Die Drehschwingungen in Kolbenmaschinen*, 1952 (Springer-Verlag, Berlin/Goettingen/Heidelberg).
19 **Rakopoulos, C. D., Giakoumis, E. G., Hountalas, D. T.,** and **Rakopoulos, D. C.** The effect of various dynamic, thermodynamic and design parameters on the performance of a turbocharged diesel engine operating under transient load conditions. SAE paper 2004-01-0926, 2004.
20 **Rakopoulos, C. D.** and **Giakoumis, E. G.** Sensitivity analysis of transient diesel engine simulation. *Proc. IMechE, Part D: J. Automobile Engineering*, 2006, **220**(D1), 89–101.
21 **Whitehouse, N. D.** and **Way, R. G. B.** Rate of heat release in diesel engines and its correlation with fuel injection data. *Proc. Instn Mech. Engrs*, 1969–1970, **184**, 17–27.
22 **Annand, W. J. D.** and **Ma, T. H.** Instantaneous heat transfer rates to the cylinder head surface of a small compression-ignition engine. *Proc. IMechE*, 1970–1971, **185**, 976–987.
23 **Meriam, J. L.** and **Kraige, L. G.** *Engineering mechanics*, dynamics, 5th edition, 2003 (Wiley, New York).
24 **Taraza, D., Henein, N.,** and **Bryzik, W.** Friction losses in multi-cylinder diesel engines. SAE paper 2000-01-0921, 2000.
25 **Teodorescu, M.** and **Taraza, D.** Combined multi-body dynamics and experimental investigation for determination of the cam-flat tappet contact condition. *Proc. Instn Mech. Engrs, Part K: J. Multi-body Dynamics*, 2004, **218**(K3), 133–142.
26 **Rakopoulos, C. D., Giakoumis, E. G.,** and **Dimaratos, A. M.** Evaluation of various dynamic issues during transient operation of turbocharged diesel engine with special reference to friction development. SAE paper 2007-01-0136, 2007.
27 **Brusa, E., Delprete, C.,** and **Genta, G.** Torsional vibration of crankshafts: effects of non-constant moments of inertia. *J. Sound Vibr.*, 1997, **205**(2), 135–150.
28 **Rakopoulos, C. D.** and **Hountalas, D. T.** A simulation analysis of a DI diesel engine fuel injection system fitted with a constant pressure valve. *Energy Convers. Manage.*, 1996, **37**, 135–150.
29 **Du, H. Y. I.** Simulation of flexible rotating crankshaft with flexible engine block and hydrodynamic bearings for a V6 engine. SAE paper 1999-01-1752, 1999.

APPENDIX

Notation

A	surface area (m^2)
b	piston acceleration (m/s^2)
BDC	bottom dead centre
C	damping coefficient (Nm s/rad)
°CA	degrees crank angle
d	shaft diameter (m)
D	cylinder bore (m)
f.m.e.p.	friction mean effective pressure (bar)
F	force (N)
g	gravitational acceleration = 9.81 m/s^2
G	mass moment of inertia ($kg\,m^2$)
k	torsional stiffness coefficient (Nm/rad), or thermal conductivity (W/m/K)
K	combustion model preparation rate constant

ℓ	shaft length (m)
L	connecting rod length (m)
N	engine speed (rpm)
p	pressure (bar)
Q	heat loss (J)
r	crank radius (m)
r/min	revolutions per minute
S	piston stroke (m)
SMD	Sauter mean diameter (μm)
t	time (s)
T	temperature (K)
TDC	top dead centre
u	velocity (m/s)
x	piston displacement (m)
β	connecting rod angle ($^\circ$)
$\Delta\varphi$	crankshaft torsional deformation ($^\circ$ or rad)
ε	angular acceleration (rad/s^2)
Θ	shear modulus (modulus of rigidity) (N/m^2)
λ	ratio of crank radius to connecting rod length
σ	torsional (shear) stress (N/m^2)
τ	torque (Nm)
φ	crank angle (deg)
ω	angular velocity (rad/s)

Subscripts

D	damping
e	engine (indicated)
fl	flywheel
fr	friction
g	gas
gr	gravitational
in	inertia
l	reciprocating
L	load, or heat loss
pist	piston
r	rotating
rod	connecting rod
S	stiffness
T	tangential
w	wall